Figure Correction of a Quartz Sub-Mirror for a Transmissive Diffractive Segmented Telescope by Reactive Ion Figuring

Qian Luo, Zhiwei Li, Xiang Wu, Junming Shao, Bin Fan, Shibin Wu, and Junfeng Du

***Abstract*— A quartz sub-mirror was figure-corrected in a parallel removal process for the first time. An Reactive Ion Figuring (RIF) process with a simple and universal masking method was demonstrated, and the 350-mm quartz sub-mirror was figure-corrected from the initial figure error of ∼23 nm RMS to the final figure error of ∼8 nm RMS in total effective figuring time of ∼52 minutes after 4 iterations, which exhibited the actual potential of RIF on the figure-correction of quartz optical elements and the possibility on applying RIF to meet the requirement of mass production for sub-mirrors of transmissive diffractive segmented telescopes.**

***Index Terms*— Reactive ion figuring, transmissive diffractive lens, figure correction, semiconductor industry, removal function, optimization algorithm.**

I. Introduction

With the increasing demand for space-based remote sensing sensitivity and resolution, space telescope aperture is becoming larger and larger [1]. Large aperture space telescope designs using transmissive diffractive optics and segmented-mirror technology have been proposed [2], [3]. Generally, a transmissive diffractive lens composed of a series of shallow and closely spaced grooves on the surface and a flat, thin underlying substrate, not a curved shape like conventional refractive and reflective components [3], [4]. Transmissive diffractive lenses can tolerate centimeter-scale ripples perpendicular to the substrate without significant focal spot distortion, which is equal to a relaxation by more than two orders of magnitude compared to a reflective component [3]. Meanwhile, optical segmented-mirror technology [5] can avoid the considerable problems encountered in the fabrication of a large, monolithic primary mirror. With the increase of the aperture of transmissive diffractive telescopes in future, for instance, up to 40 m (a similar level with E-ELT [6]), there will be thousands of segments with ∼1 m aperture requiring <20 nm RMS form accuracy and better than 1 nm RMS roughness.

So far, there has been much work on using polymer materials for improved surfaces that are compatible with substrates [7], [8]. But the fine figure correction constitutes the bottleneck stage in the optical fabricating chain. The state-of-the-art technologies like Ion Beam Figuring (IBF) [9], Magnetorheological Finishing (MRF) [10], [11] or CNC polishing processes [12], still need tens to hundreds of hours to figure a meter-class component, which arise from their insufficient throughput and the slow, point-by-point scanning removal mode, along with high cost of running and maintenance. Therefore, some alternative figuring processes mainly based on chemical removal mechanism, such as Reactive Ion Beam Etching (RIBE) [13], Plasma Jet Chemical Etching (PJCE) [14] and Reactive Atom Plasma (RAP) [15], were proposed to obtain higher material removal rate. However, the point-by-point scanning removal mode were still used in these alternative figuring processes, which means that the disadvantage of current figuring technologies for meter-class components has not yet been overcome.

Recently, a novel alternative figuring technology called Reactive Ion Figuring (RIF) with the parallel removal mode, a full-aperture tool and the chemical removal mechanism was proposed, which arose from Reactive Ion Etching (RIE) widely used in semiconductor industry for pattern transfer, combining with various masking methods.

II. Research Methodology

In this letter, a quartz sub-mirror was figure-corrected in a parallel removal process for the first time. An Reactive Ion Figuring (RIF) process with a simple and universal masking method was demonstrated. Polyimide (PI) membrane substrates have been figure-corrected by RIF to the final figure error of 17∼20 nm rms in total effective figuring time of several minutes [16], [17]. This RIF process presents the advantages of a non-contact tool combined with high material removal rate and repeatability at nanometer level, which has been proved in semiconductor industry [18]. For instance, the removal rate of PI can achieve 60 nm/min, and that of quartz can achieve 30 nm/min in conventional experiments.

As shown in Fig. 1, the reason that the RIF process can be applied to meter-class sub-mirrors is the simultaneous full-aperture tool, i.e., the aperture of the removal tool equals to

Manuscript received 11 July 2022; revised 11 August 2022; accepted 2 September 2022. Date of publication 6 September 2022; date of current version 16 September 2022. This work was supported in part by the National Key Research and Development Program of China under Grant 2016YFB0500200 and in part by the National Natural Science Foundation of China under Grant 62075220. *(Corresponding author: Qian Luo.)*

The authors are with the Institute of Optics and Electronics, Chinese Academy of Sciences, Chengdu 610209, China (e-mail: luoqian_yy@163.com; lzw@ioe.ac.cn; wuxiang21@mails.ucas.ac.cn; shaojunming2022@163.com; fanbin@ioe.ac.cn; sbwu@ioe.ac.cn; junfeng_du2012@163.com).

Color versions of one or more figures in this letter are available at https://doi.org/10.1109/LPT.2022.3204842.

Digital Object Identifier 10.1109/LPT.2022.3204842

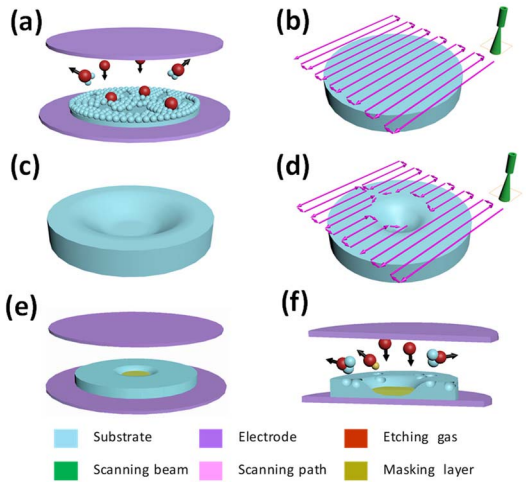

Fig. 1. Schematic of (a) the material removal mechanism of RIF; (b) the figuring mechanism of the point-by-point scanning mode; (c) a substrate with a sunken surface profile; (d) the paths of the beam spot when a sunken surface was figured by the scanning mode; (e) figuring a sunken surface by RIF; (f) cross-section of (e).

the aperture of the sample. For a 350-mm aperture mirror, the aperture of the removal tool is 350 mm; while for a 1-m aperture mirror, that is 1 m. That's because the material removal mechanism of RIF is the same as RIE: active particles reached the surface of the workpiece chemically react with atoms on the surface over the full aperture, and generated volatile products are evacuated subsequently, in which the exposed matter on the surface is removed. In a word, the removal of RIF can occur simultaneously at each point of the optical surface and be applied to typical optical materials. Considering that RIE has exhibited an excellent performance in semiconductor industries [18], RIF naturally possesses high material removal rates, nanometer-level removal accuracy and repeatability. Furthermore, different from the current point-by-point scanning figuring technologies which make use of sub-aperture tool footprint and depend on process type and spatial frequencies to correct, the material removal in RIF simultaneously occurs over the full aperture and variable distributions of masking layers are used to define protected regions and removed regions so as to remove a defined amount of material selectively according to the map of figure errors. Generally, the material removal in RIF can be described briefly as:

$$r(x,y) = \sum_{i=1}^{n} v_i(x,y) * B_i(x,y) * t_i \tag{1}$$

$$B_i(x,y) = \begin{cases} 0 & x,y \in Z_i(x,y) \\ 1 & x,y \notin Z_i(x,y) \end{cases} \tag{2}$$

where $r(x,y)$ is the removal function and represents the heights in the figure error map; $v_i(x,y)$ describes the distribution of removal rates; $B_i(x,y)$ can be called influence function which relates to the modified footprint in the ith figuring loop; t_i is the figuring time in the ith figuring loop and $Z_i(x,y)$ is the distribution of masking layers in the ith figuring loop.

Assuming that the initial surface of the preprocessed workpiece is $E_0(x,y)$, the surface of the workpiece after RIF in the nth figuring loop is $E_n(x,y)$.

$$E_n(x,y) = E_0(x,y) - \sum_{i=1}^{n} v_i(x,y) * B_i(x,y) * t_i \tag{3}$$

So the residual error of the surface after RIF in the nth figuring loop will be:

$$RMS_{E_n} = \sqrt{\frac{\sum_{n=1}^{m} [E_n(x,y) - \langle E_n \rangle]^2}{N}} \tag{4}$$

$$\langle E_n \rangle = \frac{\sum_{n=1}^{m} E_n(x,y)}{N} \tag{5}$$

Through the optimization algorithm,

$$\text{Minimize } nt$$
$$\text{Subject to } RMS_{E_n} \le C$$

where C is the threshold of RMS of the surface after RIF.

Where $t = \sum_{i=1}^{n} t_i$.

The optimal solution of the figuring time t and figuring loop n is obtained, and the distribution planning of the masking layer is optimal.

The figuring mechanism of the point-by-point scanning mode is schematically shown in Fig. 1(b). Generally speaking, the paths of the beam spot in the scanning mode have to cover the entire surface. Actually, the greatest advantage of the parallel removal mode in RIF relative to the scanning mode is the unmatched figuring efficiency for a surface with a sunken area or several pinholes shown in Fig. 1(c). If the sunken surface profile with a dozen of nanometers depth located on the surface of a meter class component requires to be figured, the figuring time using a scanning removal mode will be close to the consuming time in which a tool scans over nearly the entire surface, as shown in Fig. 1(d), for instance, dozens of hours in IBF [19]; In the contrast, the figuring time using the RIF parallel removal mode for the meter-class component will be only several minutes distributed in several loops, and there is almost no figuring time increase compared with the total figuring time of RIF for a small aperture sample. Schematics of figuring the sunken surface by RIF are shown in Fig. 1(e) and 1(f), respectively. As shown in Fig. 1(e) and 1(f), a masking layer is fabricated on the sunken area at a selected depth, and therefore, the surface region covered by the masking layer will not be influenced in this loop while the other uncovered region will be thinned in several minutes until the surface profile line reaches around the level of the masking layer.

III. Process Flow

The schematic of the RIF procedure was shown in Fig. 2, and the process of fabricating the masking layer was demonstrated in Fig. 3.

The transmitted wave-front error map of the quartz sub-mirror was measured by an interferometer in phase A. Generally, the map of transmitted wave-front errors can reveal the variation of the substrate thickness, supposing that the values of the refractive index over the full aperture have a negligible fluctuation. Therefore, the 3D map of the full aperture could be used to generate a series of 2D maps consist of thinner regions

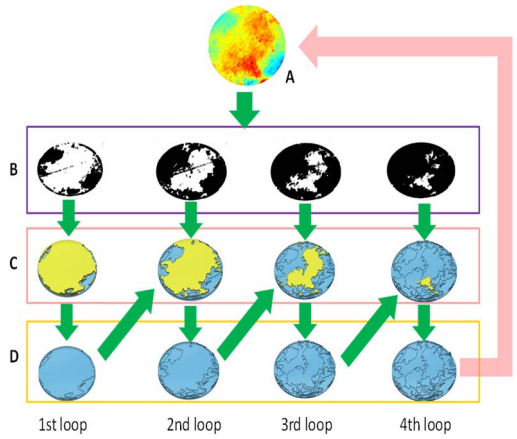

Fig. 2. Schematic of phases in RIF for the transmissive quartz element. Phase A: the transmitted wave-front map was measured; phase B: four distributions of 2D maps were simultaneously designed; phase C: the masking layers were fabricated and fixed onto the surface of the substrate; phase D: the substrate was figure-corrected and the residual masking layers were stripped.

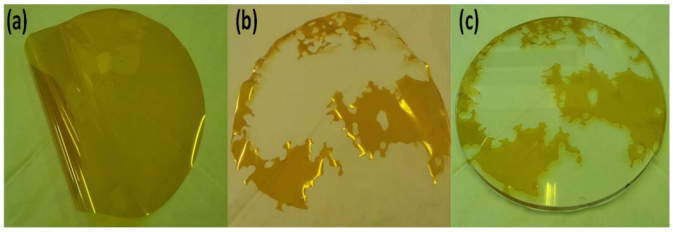

Fig. 3. Photographs of (a) a piece of PI membrane, (b) the tailored PI membrane, and (c) the fixed PI masking layer on the transmitted sub-mirror.

and thicker regions. In this schematic, four distributions of 2D maps were simultaneously produced from the initial transmitted wave-front map in phase B. In phase C, a piece of PI membrane with the same size (Fig. 3(a))as the quartz sub-mirror was first tailored to the shape of the 1st 2D map, and the parts of the PI membrane corresponding to thicker regions was cut off and stripped while those corresponding to thinner regions remained, as shown in Fig. 3(b). Subsequently, the tailored PI membrane was fixed onto the surface of the quartz element by tapes after an alignment of simple marks by mechanical parts, as shown in Fig. 3(c). Consequently, the removed regions of the designed 2D map, i.e. thicker regions, were exposed, and the protected regions of that, i.e. thinner regions, were covered by PI membrane. Next, in an RIF reactor, the material on the surface of the exposed regions was removed according to the removal amount determined in the previous design phase B, and that on the surface of the covered regions kept no change owing to the masking effect. Therefore, a fully deterministic surface figuring was achieved and the residual PI membrane was stripped in phase D after the parallel removal. Next, the flow turned to phase C of the 2nd loop from phase D of the 1st loop and a new piece of tailored PI membrane according to the 2nd 2D map was fixed onto the substrate which has been figured in the 1st loop. A distribution of protected regions and removed regions accorded with the design of the 2nd 2D map was produced onto the surface

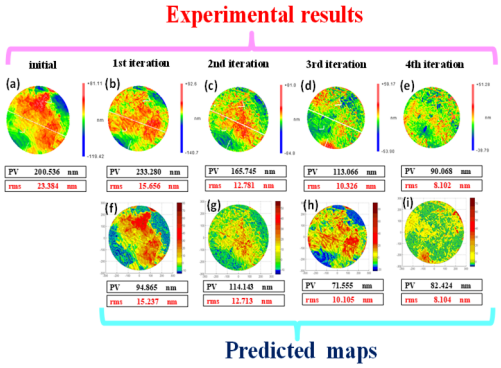

Fig. 4. Actual and simulated figuring residual errors of 350-mm effective aperture quartz substrate: (a) initial wavefront error, (b) (c) (d) (e) actual figuring residual errors in the ith figuring loop, (f) (g) (h) (i) simulated figuring residual errors in the ith figuring loop.

of the sub-mirror. Consequently, the process in each phase was implemented successively, as shown in Fig. 2, until the final loop finished, and the transmitted wave-front map of the figured sub-mirror was measured again when the flow came back to phase A. The measured result would determine whether the figure-correction procedure needed to be finished or continue with a new iteration.

The technological conditions of this experiment are as follows: the transmitted wave-front maps of the quartz substrate were measured by an interferometer (Zygo GPI600). RIF performed in a customized, 650-mm aperture capacitively coupled plasma (CCP) reactor (Beijing jinshengweina Technology Co., Ltd). The etching gases were the mixture of trifluoromethane and oxygen in a ratio of 5:1. The flowing rate of the etching gases was set to 180 sccm, the RF power was 1000 W and the chamber pressure was 1.0 Pa. The maximum removal depth was ∼300 nm in the whole figuring process and the removal rate in our experiments was ∼6 nm/min.

IV. Results and Discussions

In order to expand the application range of full-aperture plasma optical figuring technology, A 350-mm effective aperture quartz substrate was figure-corrected by RIF. The fixed threshold C is set to be less than or equal to 10nm, and the figuring loop i of A 350-mm effective aperture quartz substrate is 4 through optimization algorithm.

Taking i = 4, which means using four free-measurement iterative processes to verify the figuring methods above. A 350-mm effective aperture quartz substrate with initial wavefront error ∼23.4 nm RMS (Fig. 4(a)) is fabricated to validate the figuring performance. Fig. 4(b), Fig. 4(c), Fig. 4(d)and Fig. 4(e) show that, After 4 rounds of figuring iteration, actual figuring residual errors are ∼15.7 nm, ∼12.8nm, ∼10.3 nm and ∼8.1 nm RMS. Respectively, Fig. 4(f), Fig. 4(g), Fig. 4(h)and Fig. 4(i) show that, After 4 rounds of figuring iteration, simulated residual errors are ∼15.2 nm, ∼12.7nm, ∼10.1 nm and ∼8.1 nm RMS.

After 4 figuring iterations, the initial wavefront error of ∼23.4 nm RMS was reduced to ∼8.1 nm RMS. The mean effective figuring time per iteration was ∼13 minutes.

TABLE I
SUMMARY TABLE OF RIF RESULTS

Evaluated aspect	350 mm φ
Measurement time [min/it.]	25
Masking layer pattern design [min/it.]	10
Masking layer fabrication [min/loop]	10
Sample loading time [min/loop]	20
Mean figuring time [min/loop]	2.6
Convergence [%]	65
Figure error in rms [nm] Initial	23.4
After it. 4	8.1

The residual error map can be observed in Fig. 3(e) and a residual figure error of 8.1 nm (λ/78) RMS and 90 nm PV is obtained with a total effective figuring time of ∼52 minutes. The total effective process time in the whole procedure lasted ∼16.5 hours for an RMS convergence ratio of 65.3%. The effective figuring time means the time of removing materials by plasma in the chamber while the effective process time includes the time for measurement, pattern design, masking layer fabrication and loading. More details about the procedure steps are given in Table I.

The rapid figuring capability has been previously demonstrated on surface areas up to 350-mm diameter, which showed the actual potential for large segment class figuring. Based on the independence of the figuring time with the aperture of elements in the RIF process, the most important potential application of the RIF process is the figure correction of meter-class optical surfaces. This can be uniquely achieved by exploiting its high material removal rates, full aperture removal mode and proven nanometer-level repeatability.

V. CONCLUSION

A 350-mm quartz sub-mirror was figure-corrected in a parallel removal process for the first time. The 350-mm aperture quartz substrate was figure-corrected by RIF from the initial figure error of ∼23 nm RMS to the final figure error of ∼8 nm RMS in total effective figuring time of ∼52 minutes. Theoretically, RIF can be applied to the figure correction of flat surfaces and curved surfaces with a small rise of arch, and most of optical material can be removed easily in reactive plasma, including quartz and SiC. The simple and convenient process based on the masking layer with commercial PI film proposed in this letter can be easily applied into the figuring of other optical elements: the adaptable masking-layer-forming method would be hardly affected by the shape and material of optical elements, which simplified the masking-layer-forming process of RIF, lowered the cost of masking-layer fabrication dramatically and provided a universal solution for all kind of optical elements with various materials and shapes due to its convenience and adaptability. Depending on the simplified process, a nearly 10 hour duration for meter-class optical fabrication could be expected after a further optimization of process parameters and facilities due to the similar figuring time for mirrors with any size in RIF. The RIF of optical elements with various materials, even metal, will be investigated in future.

REFERENCES

[1] R. A. Hyde, "Eyeglass. 1. Very large aperture diffractive telescopes," *Appl. Opt.*, vol. 38, no. 19, pp. 4198–4212, Feb. 1999.

[2] M. Powers, J. Leitner, E. Hackney, K. D. Bell, and K. Schrader, "Assessment of a large aperture telescope trade space and active optomechanical control architecture," in *Proc. IEEE Aerosp. Appl. Conf.*, Snowmass, CO, USA, Feb. 1997, pp. 197–229.

[3] J. Guo, J. Zhao, L. Zhu, and D. Gong, "Status and trends of the large aperture space optical remote sensor," in *Proc. IEEE Int. Conf. Mechatronics Autom. (ICMA)*, Aug. 2018, pp. 1861–1866.

[4] P. D. Atcheson *et al.*, "MOIRE: Initial demonstration of a transmissive diffractive membrane optic for large lightweight optical telescopes," *Proc. SPIE*, vol. 8442, Sep. 2012. Art. no. 844221.

[5] D. G. Macmynowski and M. Bjorklund, "Large aperture segmented space telescope (LASST): Can we control a 12 000 segment mirror?" in *Proc. Amer. Control Conf.*, San Francisco, CA, USA, Jun. 2011, pp. 438–443.

[6] S. Jason, C. Fernando, D. Sandro, K. P. Markus, and G. Roberto, "Progress on the European extremely large telescope," *Messenger*, vol. 133, pp. 2–8, Sep. 2008.

[7] P. Maury, M. Escalante, D. N. Reinhoudt, and J. Huskens, "Directed assembly of nanoparticles onto polymer-imprinted or chemically patterned templates fabricated by nanoimprint lithography," *Adv. Mater.*, vol. 17, no. 22, pp. 2718–2723, Nov. 2005.

[8] Y. Cao *et al.*, "A transparent, self-healing, highly stretchable ionic conductor," *Adv. Mater.*, vol. 29, no. 10, Dec. 2017, Art. no. 1605099.

[9] B. Hallock, A. Shorey, and T. Courtey, "Cycle time and cost reduction in large-size optics production," *Proc. SPIE*, vol. 5869, Aug. 2005, Art. no. 58690D.

[10] S.-N. Lee, J.-I. Lee, Y.-J. Kim, and J.-G. Yook, "Low-loss thin film microstrip lines and filters based on magnetorheological finishing," *IEEE Trans. Compon. Packag. Technol.*, vol. 30, no. 4, pp. 849–854, Dec. 2007.

[11] B. Pan *et al.*, "Investigation on flatness convergence method of weak stiffness component by magnetorheological finishing," *China Mech. Eng.*, to be published.

[12] L. N. Allen and H. W. Roming, "Demonstration of an ion figuring process," *Proc. SPIE*, vol. 1333, pp. 22–33, Dec. 1990.

[13] D. Walker, "Misfit of rigid tools and interferometer subapertures on off-axis aspheric mirror segments," *Opt. Eng.*, vol. 50, no. 7, Jul. 2011, Art. no. 073401.

[14] A. Schindler *et al.*, "Precision optical asphere fabrication by plasma jet chemical etching (PJCE) and ion beam figuring," *Proc. SPIE*, vol. 4451, pp. 242–248, Dec. 2001.

[15] M. Castelli, R. Jourdain, P. Morantz, and P. Shore, "Reactive atom plasma for rapid figure correction of optical surfaces," *Key Eng. Mater.*, vol. 496, pp. 182–187, Dec. 2011.

[16] Z. W. Li *et al.*, "Highly accurate positioned, rapid figure correction by reactive ion etching for large aperture lightweight membrane optical elements," *OSA Continuum*, vol. 2, no. 12, pp. 3350–3357, Dec. 2019.

[17] Z. W. Li *et al.*, "Reactive ion figuring of large optical membrane components," *Proc. SPIE*, vol. 11568, Nov. 2020, Art. no. 115680Z.

[18] H. Abe, M. Yoneda, and N. Fujiwara, "Developments of plasma etching technology for fabricating semiconductor devices," *Jpn. J. Appl. Phys.*, vol. 47, no. 3, pp. 1435–1455, Mar. 2008.

[19] A. Chernyshev *et al.*, "Matrix based algorithm for ion-beam figuring of optical elements," *Precis. Eng.*, vol. 69, no. 16, pp. 29–35, May 2021.